

UNCLASSIFIED

AD 295 482

*Reproduced
by the*

**ARMED SERVICES TECHNICAL INFORMATION AGENCY
ARLINGTON HALL STATION
ARLINGTON 12, VIRGINIA**



UNCLASSIFIED

NOTICE: When government or other drawings, specifications or other data are used for any purpose other than in connection with a definitely related government procurement operation, the U. S. Government thereby incurs no responsibility, nor any obligation whatsoever; and the fact that the Government may have formulated, furnished, or in any way supplied the said drawings, specifications, or other data is not to be regarded by implication or otherwise as in any manner licensing the holder or any other person or corporation, or conveying any rights or permission to manufacture, use or sell any patented invention that may in any way be related thereto.

63-2-3

295482

ARL 62-457

295 482

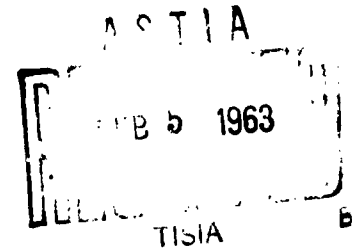
VISCOUS COMPRESSIBLE FLUID FLOW UNDER THE INFLUENCE OF A RESONANT ACOUSTIC FIELD

KENNETH R. PURDY
THOMAS W. JACKSON

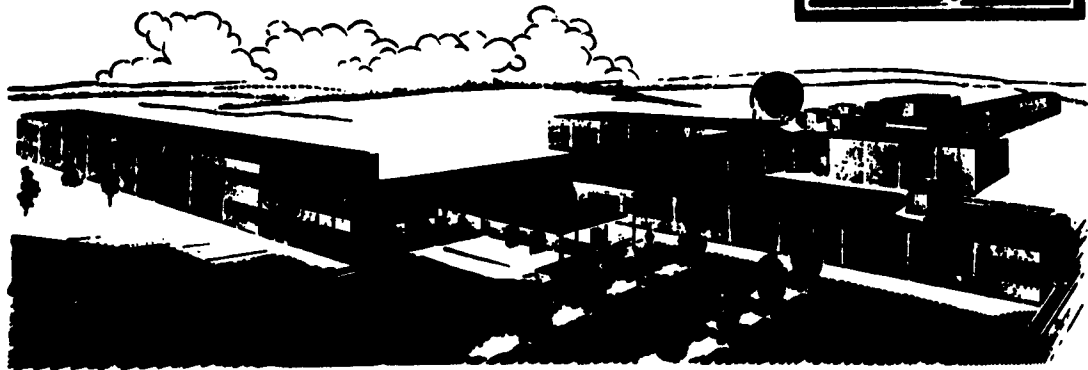
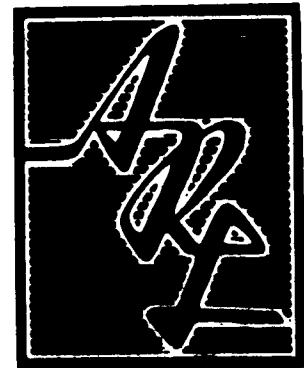
GEORGIA INSTITUTE OF TECHNOLOGY
ATLANTA, GEORGIA

OCTOBER 1962

AERONAUTICAL RESEARCH LABORATORIES
OFFICE OF AEROSPACE RESEARCH
UNITED STATES AIR FORCE



CALL FOR ASTIA
AS AD NO.



NOTICES

When Government drawings, specifications, or other data are used for any purpose other than in connection with a definitely related Government procurement operation, the United States Government thereby incurs no responsibility nor any obligation whatsoever; and the fact that the Government may have formulated, furnished, or in any way supplied the said drawings, specifications, or other data, is not to be regarded by implication or otherwise as in any manner licensing the holder or any other person or corporation, or conveying any rights or permission to manufacture, use, or sell any patented invention that may in any way be related thereto.

- - - - -

Qualified requesters may obtain copies of this report from the Armed Services Technical Information Agency, (ASTIA), Arlington Hall Station, Arlington 12, Virginia.

- - - - -

This report has been released to the Office of Technical Services, U. S. Department of Commerce, Washington 25, D. C. for sale to the general public.

- - - - -

Copies of ARL Technical Documentary Reports should not be returned to Aeronautical Research Laboratory unless return is required by security considerations, contractual obligations, or notices on a specific document.

ARL 62-457

**VISCOUS COMPRESSIBLE FLUID FLOW UNDER THE INFLUENCE
OF A RESONANT ACOUSTIC FIELD**

**Kenneth R. Purdy
Thomas W. Jackson**

**Georgia Institute of Technology
Atlanta, Georgia**

OCTOBER 1962

**Contract No. AF 33(616)-8396
Project 7063
Task 7063-01**

**AERONAUTICAL RESEARCH LABORATORIES
OFFICE OF AEROSPACE RESEARCH
UNITED STATES AIR FORCE
WRIGHT-PATTERSON AIR FORCE BASE, OHIO**

FOREWORD

This interim technical report was prepared by the School of Mechanical Engineering, Georgia Institute of Technology, Atlanta, Georgia, on contract AF 33(616)-8396 for the Aeronautical Research Laboratories, Office of Aerospace Research, United States Air Force. The report contains a summary of the results obtained from an analytical and experimental study of the influence of resonant acoustic vibrations on viscous laminar channel flow and was performed on Task 7063-01, "Research in Heat Transfer Phenomena" of Project 7063, "Mechanics of Flight". The research was administered under the technical cognizance of Dr. Max Scherberg of the Thermomechanics Research Laboratory, ARL. Dr. Scherberg's interest in the work and his many helpful suggestions are deeply appreciated.

ABSTRACT

This report presents an analytical solution for low Mach number viscous compressible channel flow under the influence of a resonant acoustic field. The solution predicts the existence of standing vortices in the flow and that the ratio of the maximum width of the vortices to the half width of the channel is solely a function of the parameter \bar{M}/M_0^2 where \bar{M} is the Mach number based on the average through flow velocity and M_0 is the acoustic Mach number based on the maximum amplitude of the time dependent velocity. The order of magnitude analysis which was used to reduce the equations of motion required that \bar{M}/M_0^2 should be less than approximately ten.

The existence of standing vortices was confirmed experimentally by a visualization study of tube flow. Typical flow fields are shown both graphically and photographically.

Finally, the threshold data of Eastwood, ARL 62-326, for convective heat transfer under the influence of a resonant acoustic field are correlated for the range of tube diameter Reynolds numbers between 11,000 and 33,000. It was shown for this case that sound affects the local heat transfer rate when \bar{M}/M_0^2 is less than 63.

TABLE OF CONTENTS

Chapter	Page
I INTRODUCTION	1
II ANALYTICAL SOLUTION FOR CHANNEL FLOW	3
III FLOW VISUALIZATION STUDY	19
IV DISCUSSION OF RESULTS	24
BIBLIOGRAPHY	27

LIST OF FIGURES

Figure	Page
1. Local Nusselt Numbers versus x/L for Various Sound Pressure Levels and 221 cps, $Re \approx 2100$	28
2. Local Nusselt Numbers versus x/L for Various Sound Pressure Levels and 216 cps, $Re \approx 11,600$	29
3. Local Nusselt Numbers versus x/L for Various Sound Pressure Levels and 222 cps, $Re \approx 49,600$	301
4. Model of Flow System	31
5. Time Dependent Velocity Profiles	32
6. Time Mean Velocity Profiles	33
7. Graphical Representation of Stream Lines	34
8. Pressure Disturbance versus Mean Through Flow Mach Number for Various Vortex Sizes	35
9. Sound Pressure Level versus Mean Through Flow Mach Number for Various Vortex Sizes	36
10. Qualitative Smoke Patterns from Preliminary Investigations for Tube Flow	37
11. Acoustic Vortices for a Resonant Rectangular Duct	38
12. Schematic Diagram of Flow Visualization Equipment	39
13. Photograph of Flow Visualization Apparatus	40
14. Typical Pressure Distribution (Frequency = 1600 cps)	41
15. Comparison of Experimental γ_S for Tube with Analytical γ_S for Channel	42

NOMENCLATURE

a	Half width of the channel	ft
c	Isentropic velocity of sound	ft/sec
c_p	Constant pressure specific heat	Btu/lb _m -°F
c_v	Constant volume specific heat	Btu/lb _m -°F
i	Square root of -1	
k	c_p/c_v	Dimensionless
L	Length of tube (References 1 and 2)	ft
M_o	Acoustic Mach number based on U_o	Dimensionless
\bar{M}	Mach number based on \bar{U}	Dimensionless
p	Pressure of a fluid	lb _f /ft ²
\bar{p}	Time mean pressure	lb _f /ft ²
p_1	Time dependent pressure	lb _f /ft ²
P_o	Average value of \bar{p} (assumed to be constant)	lb _f /ft ²
R	Gas constant	ft-lb _f /lb _m -°R
Re	Reynolds Number based on tube diameter	Dimensionless
R_s	$\pi c \lambda / v_o$	Dimensionless
s	Entropy	Btu/lb _m -°R
SPL	Sound pressure level (relative to 0.0002 microbars)	decibels
T	Absolute temperature	°R
t	Time	sec
u	x component of velocity	ft/sec
\bar{u}	Time mean component of x-velocity	ft/sec
u_1	Time dependent component of x-velocity	ft/sec
u_{10}	First approximation to u_1	ft/sec

u_{11}	Second approximation to u_1	ft/sec
U_0	Amplitude of the time dependent component of x-velocity (u_1)	ft/sec
\bar{U}	Average time mean x-velocity based on the total volume rate of flow	ft/sec
v	y-component of velocity	ft/sec
\bar{v}	Time mean component of y-velocity	ft/sec
v_1	Time dependent component of y-velocity	ft/sec
v_{10}	First approximation to v_1	ft/sec
v_{11}	Second approximation to v_1	ft/sec
X	Component of body force in the x direction	lb _f /ft ³
x	Space coordinate	ft
Y	Component of body force in the y direction	lb _f /ft ³
y	Space coordinate normal to the plane walls	ft
y^*	Dimensionless y (either α or γ)	Dimensionless
z	Space coordinate	ft

Greek Letters

α	$\beta\gamma$	Dimensionless
β	$[\omega/2 v_0]^{1/2}$	ft ⁻¹
γ	γ/a	Dimensionless
γ_s	Width of largest vortex	Dimensionless
γ_S	Maximum width of largest vortex	Dimensionless
δ	Magnitude ($\delta \ll 1$)	Dimensionless
θ	Order of magnitude	
λ	Wavelength of the acoustic vibrations	ft
μ	Dynamic viscosity of a fluid	lb _m /ft sec

ν_0	Average kinematic viscosity of a fluid	ft^2/sec
ρ	Density of a fluid	lb_m/ft^3
ρ_0	Time mean component of density	lb_m/ft^3
ρ_1	Time dependent component of density	lb_m/ft^3
ψ	Stream function (based on time mean velocity)	lb_m/sec
$\bar{\psi}$	Dimensionless stream function ($\psi/\rho_0 a \bar{U}$)	Dimensionless
ω	Circular frequency of the acoustic vibrations	rad/sec

Subscripts

x	Refers to partial differentiation with respect to x
y	Refers to partial differentiation with respect to y

CHAPTER I

INTRODUCTION

A program to study the effects of a resonant acoustic field on viscous fluid flow and convective heat transfer was initiated in the School of Mechanical Engineering of the Georgia Institute of Technology in 1958 under the sponsorship of the Aeronautical Research Laboratory at Wright Field. Since its beginning, the study [1,2] has shown that a resonant sound field had the following effects on convective heat transfer in a 4 inch ID horizontal isothermal tube:

1. For Reynolds numbers less than 33,000 the local heat transfer coefficient varied periodically with axial position in the tube. The period of this variation was one half the wavelength of the impressed resonant acoustic field. Local increases and decreases of up to 300 per cent occurred in the heat transfer coefficient with the maximum values of the local coefficient occurring at the sound particle velocity loops and the minimum values occurring at the velocity nodes. Sound threshold values, sound pressure levels below which no noticeable change in the heat transfer characteristics occurs, were found to increase with an increase in Reynolds number. Only slight increases (30 per cent) in the overall heat transfer coefficient were obtained. See Figures 1 and 2 for typical results.
2. For Reynolds numbers above 40,000 a radical change in the local characteristics took place. The resonant sound waves no longer increased the local coefficients. The local heat transfer coefficients still varied periodically with axial position and the period was the same as that for the low Reynolds number data. The position of the maximum value of the local coefficient, however, shifted to the node for the sound particle velocity and the minimum shifted to the velocity loop. This shift was also accompanied by a radical lowering of the sound threshold level. The overall heat transfer coefficient was reduced in all cases for Reynolds numbers greater than 40,000 and less than 100,000. See Figure 3 for typical results.

It should be pointed out that the tube for which the above results were obtained had a bell-mouth inlet so that the flow considered was not fully

Manuscript released by the authors September 1962 for publication as an ARL Technical Documentary Report.

developed. Calculations indicate that the boundary layer would probably be laminar for Reynolds numbers, calculated using the diameter, up to approximately 33,000. It can be concluded from the above remarks that two distinctly different phenomena exist; one characterized by laminar flow and the other by turbulent flow.

In order to achieve a better understanding of the phenomena associated with laminar flow, an analytical investigation of viscous compressible channel flow under the influence of a resonant acoustic field was initiated. The results of this analytical study are presented herein. Preliminary results of a qualitative visualization study of tube flow are also presented in support of the analytical interpretations.

CHAPTER II

ANALYTICAL SOLUTION FOR CHANNEL FLOW

A. Theoretical Considerations

The problem is that of determining analytically the velocity field which is formed by imposing a resonant acoustic field with a circular frequency, ω , upon a compressible fluid flowing between infinite parallel walls separated by a distance $2a$. The mathematical model is shown in Figure 4. The flow is assumed to be independent of the z direction. Thus the velocity of the fluid is dependent upon position as given by x and y and upon time, t . For this model the equations which govern the fluid motion are

Continuity

$$\rho_t + (\rho u)_x + (\rho v)_y = 0 \quad \dots(1)$$

Momentum

$$\begin{aligned} \rho(u_t + u \cdot u_x + v \cdot u_y) &= X - p_x + \\ &[\mu(2 u_x - \frac{2}{3}\{u_x + v_y\})]_x + \\ &[\mu(u_y + v_x)]_y \end{aligned} \quad \dots(2a)$$

and

$$\begin{aligned} \rho(v_t + u \cdot v_x + v \cdot v_y) &= Y - p_y + \\ &[\mu(2 v_y - \frac{2}{3}\{u_x + v_y\})]_y + \\ &[\mu(u_y + v_x)]_x \end{aligned} \quad \dots(2b)$$

B. Assumptions

In order to reduce the above equations to a form which can be solved, the following assumptions are made:

1. It is assumed that the pressure may be written as the sum of a time mean component $\bar{p}(x,y)$ and a time dependent component $p_1(x,t)$ which is independent of the y -direction. It is further assumed that $p_1(x,t)$ is directly related to the resonant acoustic field and, therefore, it is periodic in both time, t , and position, x . Thus

$$p(x, y, t) = \bar{p}(x, y) + p_1(x, t) \quad \dots(3)$$

2. Since the pressure is assumed to consist of a time mean component and a periodic component it is plausible to assume that the density may also be represented in this fashion. However, spacial variations in the density are assumed to have only a small effect upon the flow and, therefore, the time mean of the density, $\bar{\rho}(x, y)$, is considered to be constant and equal to ρ_0 . Thus

$$\rho(x, y, t) = \rho_0 + \rho_1(x, t) \quad \dots(4)$$

3. The viscosity of the fluid is assumed to be constant and equal to μ_0 .
4. Following Lin [3], it is assumed that the x -velocity component, $u(x, y, t)$, and the y -velocity component, $v(x, y, t)$, may be separated into time mean and periodic components as follows:

$$u(x, y, t) = \bar{u}(x, y) + u_1(x, y, t) \quad \dots(5)$$

$$v(x, y, t) = \bar{v}(x, y) + v_1(x, y, t) \quad \dots(6)$$

$$\text{where } \bar{u}_1 = \bar{v}_1 \equiv 0 \quad \dots(7)$$

5. No body forces are assumed to be present.
i.e.

$$X = Y = 0 \quad \dots(8)$$

6. The continuity and momentum equations can be written in dimensionless form by assuming the following change of variables:

$$u' = u/U_0 = \bar{u}' + u_1' \quad \dots(9a)$$

$$v' = v/U_0 = \bar{v}' + v_1' \quad \dots(9b)$$

$$x' = x/\lambda \quad \dots(9c)$$

$$y' = y/\lambda \quad \dots(9d)$$

$$p' = p/\rho_0 U_0^2 = \bar{p}' + p_1' \quad \dots(9e)$$

$$\rho' = \rho/\rho_0 = 1 + \rho_1' \quad \dots(9f)$$

$$\mu' = \mu/\mu_0 \quad \dots(9g)$$

$$t' = t/(\lambda/U_0) \quad \dots(9h)$$

7. The order of magnitude of each of the dimensionless quantities is assumed to be

$$x' = \theta(1) \quad \dots(10a)$$

$$y' = \theta(\delta) \quad \dots(10b)$$

$$u_1' = \theta(1) \quad \dots(10c)$$

$$\bar{u}' = \theta(\delta) \quad \dots(10d)$$

$$v_1' = \theta(\delta) \quad \dots(10e)$$

$$\bar{v}' = \theta(\delta^2) \quad \dots(10f)$$

$$\rho_1' = \theta(\delta) \quad \dots(10g)$$

C. Reduced Equations

Continuity

The dimensionless continuity equation can be reduced by retaining only the terms which are of order one. This yields the following dimensional equation

$$\rho_{1_t} + \rho_0 \cdot u_{1_x} + \rho_0 v_{1_y} = 0 \quad \dots(11)$$

Taking the time average over one period yields

$$\bar{u}_x + \bar{v}_y = -\frac{1}{\rho_0} \overline{\{\rho_1 \cdot u_{1_x} + \rho_1 \cdot v_{1_y} + u_1 \cdot \rho_{1_x}\}} \quad \dots(12)$$

Momentum

The dimensionless momentum equation can be reduced by

- (1) eliminating the pressure between the x and y equation by noting that $p_{xy} = p_{yx}$,
- (2) assuming the Reynolds number, $\rho_0 U_0 \lambda / \mu_0$, is of order $1/b^2$, and
- (3) retaining only the terms that are of order $1/b$ or larger, or
- (4) taking the time average and retaining only the terms that are of order one or greater.

Conditions (1), (2) and (3) reduce the momentum equations to

$$v_0 u_{1_{yyy}} = [u_{1_t} + u_1 \cdot u_{1_x} + v_1 \cdot u_{1_y}]_y \quad \dots(13)$$

Conditions (1), (2) and (4) reduce the momentum equations to

$$v_0 \bar{u}_{yyy} = Q_y \quad \dots(14)$$

where

$$Q = \overline{\left\{ u_1 \cdot u_{1x} + v_1 \cdot u_{1y} + \frac{\rho_1}{\rho_0} \cdot u_{1t} + \frac{\rho_1}{\rho_0} u_1 \cdot u_{1x} + \frac{\rho_1}{\rho_0} v_1 \cdot u_{1y} \right\}} \quad \dots(15)$$

Summary of the Reduced Equations

(1) For $u_1(x, y, t)$ and $v_1(x, y, t)$

$$\text{Continuity} \quad u_{1x} + v_{1y} = (1/\rho_0) \rho_{1t} \quad \dots(16)$$

$$\text{Momentum} \quad v_0 u_{1yyy} = [u_{1t} + u_1 \cdot u_{1x} + v_1 \cdot u_{1y}] \quad \dots(17)$$

The solution to the above equations must satisfy the following boundary conditions:

$$u_1 = v_1 = 0 \text{ at } y = 0 \quad \dots(18a)$$

$$u_{1y} = 0, v_1 = 0 \text{ at } y = a \quad \dots(18b)$$

$$u_1 = -U_0 \cos(\omega t), \text{ at } x = 0, y = a \quad \dots(18c)$$

The first and second conditions are required by no-slip and symmetry respectively. The third condition is imposed by the assumed acoustic field. Sanders [4] has shown experimentally that outside a very thin layer of fluid near the walls the velocity is the same, at least to a first approximation, as that of an inviscid compressible fluid undergoing resonant acoustic vibrations.

(2) For $\bar{u}(x, y)$ and $\bar{v}(x, y)$

$$\text{Continuity} \quad \bar{u}_x + \bar{v}_y = -1/\rho_0 \overline{\left\{ \rho_1 \cdot u_{1x} + \rho_1 \cdot v_{1y} + u_1 \cdot \rho_{1x} \right\}} \quad \dots(19)$$

$$\text{Momentum} \quad v_0 \bar{u}_{yyy} = Q_y \quad \dots(20)$$

The solution to the above equations must satisfy the following boundary conditions:

$$\bar{u} = \bar{v} = 0 \text{ at } y = 0 \quad \dots(21a)$$

$$\bar{u}_y = 0, \bar{v} = 0 \text{ at } y = a \quad \dots(21b)$$

$$\int_0^a \rho_0 \bar{u} dy = \rho_0 a \bar{U} = \text{constant for all } x \quad \dots(21c)$$

The first two conditions are again no-slip and symmetry respectively. The third condition requires steady time mean flow and forms the basic difference between this study and the previous studies of Rayleigh [5] and Westervelt [6] who treated the special case of no through flow.

The solutions of these equations will be outlined in detail since the underlying assumptions are not clearly defined in the existing literature.

D. Solution for the Time Dependent Velocity

A solution to Equations 16, 17 and 18 can be obtained by the method of successive approximations [7], i.e., the velocities $u_1(x, y, t)$ and $v_1(x, y, t)$ are assumed to consist of two terms such that

$$u_1(x, y, t) = u_{10}(x, y, t) + u_{11}(x, y, t) \quad \dots(22)$$

$$v_1(x, y, t) = v_{10}(x, y, t) + v_{11}(x, y, t) \quad \dots(23)$$

where the first approximations, u_{10} and v_{10} are the solution of

$$\text{Continuity} \quad u_{10_x} + v_{10_y} = (-1/\rho_0) \rho_{1_t} \quad \dots(24)$$

$$\text{Momentum} \quad v_0 u_{10_{yy}} = u_{10_t} + F(x, t) \quad \dots(25)$$

Equation 25 is the result of integrating Equation 17 with respect to y . It can also be obtained from an order of magnitude analysis of the dimensionless

form of Equation 2a. This analysis shows that $F(x, t) = \frac{1}{\rho_0} p_{1x}$.

The second approximations, u_{11} and v_{11} , are the solution of

$$\text{Continuity } u_{11x} + v_{11y} = 0 \quad \dots(26)$$

$$\text{Momentum } u_{11t} - v_0 u_{11yy} = -u_{10} \cdot u_{10x} - v_{10} \cdot u_{10y} \quad \dots(27)$$

The solutions to the above equations must satisfy the following boundary conditions:

$$u_{10} = u_{11} = v_{10} = v_{11} = 0 \text{ at } y = 0 \quad \dots(28a)$$

$$u_{10y} = u_{11y} = v_{10} = v_{11} = 0 \text{ at } y = a \quad \dots(28b)$$

$$u_{10} = -U_0 \cos(\omega t), u_{11} = 0 \text{ at } y = a, x = 0 \quad \dots(28c)$$

First Approximations

In addition to the seven assumptions given previously the following assumptions are made:

8. It is assumed that all quantities which are periodic in time are proportional to $\exp(-i\omega t)$, i.e

$$f(x, y, t) = f_1(x, y) \cdot \exp(-in\omega t) \quad \dots(29)$$

$$\text{where } n = 1, 2, 3, \dots \quad \dots(30)$$

9. The time dependent component of pressure, $p_1(x, t)$, is assumed to be the same as the pressure in a stationary inviscid fluid which is undergoing resonant acoustic vibrations. Morse [8] gives this as

$$p_1(x, t) = -i \rho_0 c U_0 \sin(\omega x/c) \exp(-i\omega t) \quad \dots(31)$$

10. It is further assumed that the form of the first approximation to the x-velocity, u_1 , is

$$u_{10}(x, y, t) = U_0 \cos\left(\frac{\omega x}{c}\right) F_1(y) \exp(-i\omega t) \quad \dots(32)$$

This form is selected since Sanders [4] has shown that a real fluid undergoing resonant acoustic vibrations has the same velocity as an inviscid fluid outside a very thin layer of fluid near the stationary boundary. The velocity for an inviscid fluid, as given by Morse[8], is

$$u_1(x, t) = -U_0 \cos\left(\frac{\omega x}{c}\right) \exp(-i\omega t) \quad \dots(33)$$

Thus the fact that the fluid is viscous is assumed to affect only the amplitude and the phase of the velocity and to be solely a function of y , namely $F_1(y)$.

11. Finally, in order to eliminate $\rho_1(x, t)$ from the above equations, it is necessary to assume a relationship between the pressure and the density of the fluid. The pressure-density variation due to the time mean flow, i.e. due to $\bar{p}(x, y)$ and $\bar{T}(x, y)$, will be omitted from this analysis and only the relationship between pressure and density during the compressions and rarefactions of the fluid will be considered. To achieve this it is assumed that

- (a) The fluid is a perfect gas, i.e.

$$\rho = \frac{P}{RT}, \quad c_p = \text{Constant}; \text{ and}$$

- (b) The compression-rarefaction process is isentropic, i.e.

$$p\rho^{-k} = \text{Constant}, \text{ where } k = c_p/c_v.$$

The wave propagation speed, c , for isentropic compressions and rarefactions is given by

$$c^2 = \left. \frac{\partial p}{\partial \rho} \right|_s = k \frac{p}{\rho} \quad \dots(34)$$

From these assumptions and the further assumption that $p_1/\bar{p} = \theta(\delta)$, the following relationship can be shown

$$p_1 \approx c^2 \rho_1 \quad \dots(35)$$

Under the above assumptions Equation 25 reduces to

$$\{F_1'' + i\omega/v_0 F_1 + i\omega/v_0\} U_0 \cos(\omega x/c) \exp(-i\omega t) = 0 \quad \dots(36)$$

For this to be satisfied in general the equation in brackets must be equal to zero, i.e.

$$F_1'' + i\omega/v_0 F_1 = -i\omega/v_0 \quad \dots(37)$$

The general solution for $F_1(y)$ is

$$F_1(y) = -1 + A \exp[\beta(1-i)y] + B \exp[-\beta(1-i)y] \quad \dots(38)$$

where $\beta \equiv \sqrt{\omega/2 \cdot v_0}$

or finally

$$u_{10}(x, y, t) = U_0 \cos(\omega x/c) \{-1 + A \exp[\beta(1-i)y] + B \exp[-\beta(1-i)y]\} \quad \dots(39)$$

The y component of velocity, v_{10} , can now be determined from Equation 24 since $\rho_1(x, t)$ and $u_{10}(x, y, t)$ are known. Upon applying the appropriate boundary conditions to the real parts of u_{10} and v_{10} , the following solution is obtained:

$$u_{10}(x, y, t) = -U_0 \cos(\omega x/c) [\cos(\omega t) - \exp(-\beta y) \cdot \cos(\omega t - \beta y)] \quad \dots(40)$$

$$v_{10}(x, y, t) = \frac{U_0 \omega}{\sqrt{2}\beta c} \sin(\omega x/c) [\cos(\omega t - \pi/4) - \exp(-\beta y) \cdot \cos(\omega t - \beta y - \pi/4)] \quad \dots(41)$$

The first approximations to u_1 and v_1 given above are the same as those given by Westervelt [6].

Second Approximations

The following equation is the result of substituting the complex form of Equations 40 and 41 into Equation 27:

$$u_{11t} - v_0 u_{11yy} = \frac{\omega U^2}{2c} \sin(2\omega x/c) \cdot \{1 - \exp(-\beta[1-i]y)\} \exp(-2i\omega t) \quad \dots(42)$$

Another assumption is now necessary.

12. It is assumed that the form of $u_{11}(x, y, t)$ is given by

$$u_{11}(x, y, t) = \frac{\omega U^2}{2c v_0} \sin(2\omega x/c) F_2(y) \cdot \exp(-i2\omega t) \quad \dots(43)$$

The above assumption is based upon the premise that the convective terms give rise to higher harmonics in both position and time.

Substituting Equation 43 into Equation 42 produces a linear total differential equation in $F_2(y)$. The solution of Equations 26 and 42 under the restraints of Equations 28 is

$$u_{11}(x, y, t) = \frac{U^2}{4c} \sin(2\omega x/c) \{ \sin(2\omega t) + \exp(-\sqrt{2}\beta y) \cdot \sin(2\omega t - \sqrt{2}\beta y) - 2 \exp(-\beta y) \cdot \sin(2\omega t - \beta y) \} \quad \dots(44)$$

and

$$v_{11}(x, y, t) = -\frac{\omega U^2}{2\beta c^2} \cos(2\omega x/c) \{ \beta y \sin(2\omega t) + (\sqrt{2} - 1/2) \cos(2\omega t + \pi/4) + 1/2 \exp(-\sqrt{2}\beta y) \cdot \cos(2\omega t - \sqrt{2}\beta y + \pi/4) - \sqrt{2} \exp(-\beta y) \cdot \cos(2\omega t - \beta y + \pi/4) \} \quad \dots(45)$$

Dimensionless Velocity Components

The following two equations represent the time dependent components of velocity, u_1 and v_1 , in dimensionless form to a second approximation:

$$u_1'(x', y', t') = -\cos(2\pi x') \{ \cos(2\pi t'/M_0) - \exp(-\sqrt{R_s} y') \cos(2\pi t'/M_0 - \sqrt{R_s} y') \} + (M_0/4) \cdot \sin(4\pi x') \{ \sin(4\pi t'/M_0) + \exp(-\sqrt{2R_s} y') \cdot \sin(4\pi t'/M_0 - \sqrt{2R_s} y') - 2 \exp(-\sqrt{R_s} y') \cdot \sin(4\pi t'/M_0 - \sqrt{R_s} y') \} \dots (46)$$

and

$$v_1'(x', y', t') = (\sqrt{2} \pi / \sqrt{R_s}) \sin(2\pi x') \cdot \{ \cos(2\pi t'/M_0 - \pi/4) - \exp(-\sqrt{R_s} y') \cdot \cos(2\pi t'/M_0 - \sqrt{R_s} y - \pi/4) \} - (\pi / \sqrt{R_s}) M_0 \cos(4\pi x') \{ \sqrt{R_s} y' \sin(4\pi t'/M_0) + (\sqrt{2} - 1/2) \cos(4\pi t'/M_0 + \pi/4) + 1/2 \exp(-\sqrt{2R_s} y') \cdot \cos(4\pi t'/M_0 - \sqrt{2R_s} y' + \pi/4) - \sqrt{2} \exp(-\sqrt{R_s} y') \cdot \cos(4\pi t'/M_0 - \sqrt{R_s} y' + \pi/4) \} \dots (47)$$

where

$$R_s \equiv \frac{\pi c \lambda}{v_0} \dots (48)$$

and

$$M_0 = \frac{1}{k} (p_1/p_0) \dots (49)$$

The above solution is valid only if the original order of magnitude assumptions are satisfied. Therefore, the following restrictions are required:

$$(a) M_0 = \theta(\delta) \text{ or } p_1/p_0 = \theta(\delta) \quad \dots(50)$$

$$(b) R_s = \theta(1/\delta^2) \quad \dots(51)$$

The first requirement was also necessary in the development of Equation 35. The second requirement is satisfied by gases at normal pressures and temperatures and for wavelengths which are greater than approximately 6 inches.

It can also be seen that the contribution of the second approximation is directly proportional to the magnitude of the pressure disturbance.

Under the order of magnitude assumptions and for the range of frequency that was investigated experimentally (600 to 1600 cps), it can be shown numerically that the second approximation can be neglected. Therefore, the analysis of the time mean flow will be based on the first approximation to the time dependent velocity, u_{10} . $u_1(0, y', t')$ is shown in Figure 5.

E. Time Mean Velocities

The primary characteristics of the time mean flow can be determined by considering only the first approximation to u_1 and v_1 , i.e. Equations 40 and 41. A further assumption is, however, necessary.

13. The terms $\frac{\rho_1}{\rho_0} u_1 \cdot u_{1x}$ and $\frac{\rho_1}{\rho_0} v_1 \cdot u_{1y}$ will be neglected since they yield terms which are higher harmonics in both time and position.

Therefore, to a first approximation

$$Q = u_{10} \cdot u_{10x} + v_{10} \cdot u_{10y} + \frac{\rho_1}{\rho_0} u_{10t} \quad \dots(52)$$

or upon substituting Equations 40 and 41 into Equation 52

$$Q = -\frac{\omega U_0^2}{4c} \sin(2\omega x/c) \{ 2 - \exp(-\beta y) \cdot [3 \cos(\beta y) - \sin(\beta y)] + \exp(-2\beta y) \} \quad \dots(53)$$

Equation 20 can now be solved for $\bar{u}(x, y)$ as follows:

Substitution of Equation 53 into Equation 20 yields

$$\bar{u}_{yyy} = \frac{\omega U_0^2}{4c v_0} \sin(2\omega x/c) \left\{ \frac{\partial}{\partial y} [\exp(-\beta y) \cdot (3 \cos\{\beta y\} - \sin\{\beta y\}) - \exp(-2\beta y)] \right\} \quad \dots(54)$$

Equation 54 is a linear partial differential equation of the form

$$\bar{u}_{yyy} = f(x) \cdot g(y) \quad \dots(55)$$

for which the solution is

$$\bar{u}(x, y) = f(x) \int_0^y \int_0^{y'} \int_0^{y''} g(y) dy' dy'' dy''' + F_3(x) \frac{y^2}{2} + F_4(x)y + F_5(x) \quad \dots(56)$$

or

$$\bar{u}(x, y) = \frac{U_0^2}{8c} \sin(2\omega x/c) \{ -4(\beta y)^2 + 2\beta y + 3 - \exp(-\beta y) [2 \cos(\beta y) + 6 \sin(\beta y) + \exp(-\beta y)] \} + F_3(x) \cdot y^2/2 + F_4(x) \cdot y + F_5(x) \quad \dots(57)$$

From the no-slip condition, $F_5(x) = 0$, the y component of velocity, \bar{v} , can now be determined from continuity, Equation 19. This yields

$$\bar{v}_y = -\frac{U_0^2}{4c^2} \cos(2\omega x/c) \{ -4(\beta y)^2 + 2\beta y + 3 - \exp(-\beta y) [2 \cos(\beta y) + 7 \sin(\beta y)] - \exp(-2\beta y) \} + \frac{U_0^2}{4c^2} \exp(-\beta y) \sin(\beta y) - F_3'(x) \frac{y^2}{2} - F_4'(x) y \quad \dots(58)$$

which, when integrated with respect to y and subjected to the no-slip condition, becomes

$$\begin{aligned} \bar{v}(x, y) = & -\frac{U_0^2}{8\beta c^2} \left\{ \left[-\frac{8}{3}(\beta y)^3 + 2(\beta y)^2 + 6\beta y - 10 + \right. \right. \\ & \left. \left. \exp(-\beta y)\{9 \cos(\beta y) + 5 \sin(\beta y)\} + \exp(-2\beta y) \right] \cos(2\omega x/c) + \right. \\ & \left. \exp(-\beta y)\{\cos(\beta y) + \sin(\beta y)\} - 1 \right\} - F_3'(x) y^3/6 - F_4'(x) y^2/2 \quad \dots(59) \end{aligned}$$

If $F_3(x)$ and $F_4(x)$ are determined from the boundary conditions given in Equations 21b and 21c, then the time mean velocities in dimensionless form become

$$\begin{aligned} \bar{u}'(x', y') = & 3(\bar{U}/U_0)[\gamma - \gamma^2/2] - (M_0/8) \sin(4\pi x') \cdot \\ & \left\{ \left[9 - \frac{27}{2\beta a} \right] [\gamma - \gamma^2/2] - 3 + \exp(-\alpha) \cdot \right. \\ & \left. [2 \cos(\alpha) + 6 \sin(\alpha) + \exp(-\alpha)] \right\} \quad \dots(60) \end{aligned}$$

and

$$\begin{aligned} \bar{v}'(x', y') = & - (M_0\pi/4)(a/\lambda) \{ \cos(4\pi x') [\{ 9 - \frac{27}{2\beta a} \} \{ \gamma^3/3 - \gamma^2 \} + \\ & 6\gamma - 10/\beta a + (1/\beta a) \exp(-\alpha) \cdot \{ 9 \cos(\alpha) + 5 \sin(\alpha) + \exp(-\alpha) \}] + \\ & (1/\beta a) \exp(-\alpha) \{ \cos(\alpha) + \sin(\alpha) - 1/\beta a \} \quad \dots(61) \end{aligned}$$

where $\gamma \equiv y/a$ and $\alpha \equiv \beta y$

For gases at normal pressures and temperatures $\beta \gg 1$ and, therefore, $1/\beta a \ll 1$ and can be neglected.

The above solution further clarifies the order of magnitude assumptions since if the above solution is valid then

$$(a) \quad \bar{U}/U_0 = \theta(\delta) \quad \text{or} \quad \bar{M}/M_0 = \theta(\delta) \quad \dots(62)$$

$$(b) \quad M_0 = \theta(\delta) \quad \text{which from (a) yields} \quad \dots(63)$$

$$\bar{M} = \theta(\delta^2) \quad \dots(64)$$

and

$$(c) \quad a/\lambda = \theta(\delta) \quad \dots(65)$$

The x component of the time mean velocity profile is shown in Figure 6 for selected values of x' .

F. Stream Function

If the spacial variations in the time mean density are neglected then an expression for the stream function can be determined as follows:

$$\psi(x', y^*) = \psi(x', 0) + \int_0^{y^*} \rho_0 \bar{u}(x', z) dz \quad \dots(66)$$

If $\psi(x', 0) = 0$ then $\psi(x', y)$ becomes

$$\begin{aligned} \bar{\psi}(x', y^*) \cong \psi(x', y^*)/\rho_0 a \bar{u} &= \frac{3}{2}(\gamma^2 - \gamma^3/3) + (M_0^2/\bar{M}) \sin(4\pi x') \cdot \\ &\left\{ -\frac{9}{2} \left[1 - \frac{3}{2\beta a} \right] [\gamma^2 - \gamma^3/3] + 3\gamma + (1/2\beta a) [\exp(-\alpha) \cdot \right. \\ &\left. \{ 8 \cos(\alpha) + 4 \sin(\alpha) + \exp(-\alpha) \} - 9] \right\} \quad \dots(67) \end{aligned}$$

Figure 7 is a graphical representation of Equation 67 for selected values of a , λ , \bar{M} and M_0 .

If only one half of the flow shown in Figure 7 is considered then there are three vortices for each increment of length, $\lambda/2$. Two of the vortices are very thin and would be undetected in flow visualization studies. However, the third vortex can completely fill the half width of the channel if the through flow is reduced to zero. This condition would also produce a fourth vortex. An approximate expression can be determined for the size, γ_s , of this vortex in its visible range since $\exp(-\alpha) \approx 0$ and also $1/\beta a \approx 0$. The size, γ_s , is simply the largest positive root of $\psi(x', y^*) = 0$. Under the above simplifications γ_s becomes

$$\gamma_s = \frac{3}{2} - \left\{ \frac{9}{4} - 2/[1 - \frac{8\bar{M}}{3M_0^2} \csc(4\pi x')] \right\}^{1/2} \quad \dots(68)$$

The maximum value of γ_s , γ_S , occurs when $x' = (4m-1)/8$; $m = 1, 2, 3, \dots$.

γ_S becomes

$$\gamma_S = \frac{3}{2} - \left\{ \frac{9}{4} - 2/[1 + (8\bar{M}/3M_0^2)] \right\}^{1/2} \quad \dots(69)$$

Thus the maximum size of a vortex is solely a function of the dimensionless parameter \bar{M}/M_0^2 . The order analysis, however, restricts the region over which Equation 69 is applicable since (a) $M_0 = \theta(b)$ and (b) $\bar{M}/M_0 = \theta(b)$. If conditions (a) and (b) are combined then $\bar{M}/M_0^2 = \theta(1)$.

The pressure disturbance necessary to produce a given size vortex is

$$p_1/p_0 = 2k \left\{ \frac{2\bar{M}}{3} \left[\frac{9 - (3 - 2\gamma_S)^2}{(3 - 2\gamma_S)^2 - 1} \right] \right\}^{1/2} \quad \dots(70)$$

or in terms of sound pressure level (relative to 0.0002 microbars)

$$\begin{aligned} \text{SPL} = 134 + 8.6858 \ln \left[\frac{2k p_0}{2.95429} \cdot \right. \\ \left. \left\{ \frac{2\bar{M}}{3} \left[\frac{9 - (3 - 2\gamma_S)^2}{(3 - 2\gamma_S)^2 - 1} \right] \right\}^{1/2} \right] \text{db} \quad \dots(71) \end{aligned}$$

Figures 8 and 9 are the graphical representations of Equations 70 and 71 respectively.

CHAPTER III

FLOW VISUALIZATION STUDY

A. Geometry

Before the analytical study presented in Chapter II was initiated a preliminary flow visualization study was conducted to determine whether or not a resonant acoustic field would produce a time-mean secondary flow. Since the heat transfer experiments had been conducted for a circular tube it seemed logical to use a circular tube for the preliminary flow visualization study. The first results of this study (these are qualitative only) demonstrated that secondary time-mean-flow does exist and that the flow seemed to be periodic with respect to axial position with a period equal to one half the wavelength of the impressed standing wave field. The flow patterns are shown in Figure 10.

This study also showed that when secondary flows were present the average through-flow velocity was small in comparison to the velocity of a fluid particle at a velocity loop in the standing wave field. It also indicated that the pressure disturbance was small in comparison to the time-mean pressure. These observations, the analyses of Rayleigh [5], Westervelt [6], and Schlichting [7] and the flow visualization studies of Andrade [9] formed the basis of the analysis which are presented in Chapter II.

It was originally anticipated that a study of the two-dimensional channel would produce the simplest experimental system. Consequently, the theoretical work was based upon the infinite parallel plate geometry. This geometry also afforded a check on Rayleigh's solution for the special case of no through flow.

A preliminary investigation of a rectangular duct verified the premise that standing vortices could also be produced in this flow. A typical vortex is

shown in Figure 11. However, this geometry from an experimental aspect has many disadvantages. Several of these are discussed below.

1. In order to improve a flow visualization apparatus from one which simply verifies the existence of standing vortices to one which will yield quantitative data, a great deal of care must be taken in the design to be certain that the actual flow is representative of the postulated channel flow. Since a side boundary layer is formed in a rectangular duct, the duct width to height ratio should be quite large so that the side boundary layer effects can be neglected.
2. In order to verify the analytical solution, the easiest parameter to measure is the size of the vortices. This should be solely a function of \bar{M}/M_0^2 . Accurate measurements from photographs require a duct height of at least 0.5 inch. Consequently, a duct width of at least 5 to 10 inches is required.
3. In order to supply the large quantities of acoustic power required with a simple driver-horn system, the horn should also be at least 0.5 inch in diameter. This in turn limits the minimum frequency to approximately 1,000 cps and yields a sound wavelength for an open duct in normal atmospheric air to about 14 inches. Thus the duct width is of the same order of magnitude as the sound wavelength.
4. In order to have plane wave propagation, it is necessary that the largest cross sectional duct dimension be small in comparison to the wavelength. Thus a contradiction in requirements has resulted. The easiest requirement to relax is the duct width. However, it is then questionable whether or not the data will be of quantitative value.
5. In order to overcome the above difficulties a new method of producing the sound field would have to be devised.

If the same factors are considered for a circular tube then it is found that no outstanding difficulties exist other than relating the quantitative results for a tube to the analytical solution for a channel. Circular tube flow is axially symmetric (no extraneous side boundary layer effects). Also, the tube diameter can be made small in comparison to the sound wavelength without sacrificing accuracy in the vortex measurements.

On the premise that the vortex size should be a function of the same parameter \bar{M}/M_0^2 for both a circular tube and channel flow, it was decided to attempt to perfect the circular tube geometry in order to obtain quantitative flow visualization data.

B. Apparatus

The experimental apparatus consisted of the following items:

1. Test Section. The test section was composed of an inlet plenum chamber and a 1 inch ID Pyrex glass tube 42 inches long. For the air pressure and temperature that was maintained, the fundamental resonant frequency for this tube was 160 cps. The inlet end of the tube was flared to form a bellmouthed entrance. Primary air was admitted to the inlet plenum from a small calming chamber. The air flow was directed up and to the rear of the inlet plenum. This permitted sufficient residence time for the air to reach thermal equilibrium with the system and also prevented appreciable distortion in the velocity profile at the tube inlet.

Smoke was also admitted to the inlet plenum. However, the smoke was added periodically to this chamber and allowed to mix with the steady flow of primary air. The smoke remained in the inlet plenum long enough to be completely mixed with the air and a charge of smoke often lasted for more than 20 minutes. The air-smoke mixture was discharged from the tube into an exit plenum which was provided with an exhaust blower and duct. The test section was housed in an acoustic shield to reduce the sound level in the laboratory and also to eliminate extraneous light. The entire system is shown schematically in Figure 12 and photographically in Figure 13.

2. Light Source. Two light sources were used in this study; a 400 watt mercury vapor lamp and a flash tube which produced a 200 watt-second line source. The flow was illuminated by directing the light beam down the tube from the inlet end. Either two collimating slits were used to produce a light beam to illuminate a vertical plane of fluid through the axis of the tube or the beam was allowed to illuminate the entire tube.
3. Air and Smoke Supply. A variable speed Roots blower supplied low pressure atmospheric air to the system. The air was taken directly from the air conditioned laboratory. The thermal inertia of the system was sufficient to damp small oscillations in the room temperature. Since a positive displacement blower was used it was necessary to insert a storage tank in the supply line to damp the low frequency flow pulsations. The air flow from the storage was measured with a dry gas meter and it was then split into a primary air stream and a secondary stream to supply air to either a tobacco smoker or to an oil vaporizer. The two streams were united again in the inlet plenum chamber. The flow patterns were qualitatively the same for both the oil and the tobacco smoke. The oil unit was much less trouble to use and, therefore, it constituted the primary source of smoke for the system. Large variations in the ratio of smoke to air did not appear to affect the flow patterns, unless extremely large amounts of smoke were used.
4. Sound Generating Equipment. A Hewlett-Packard Model 206A audio signal generator provided a source of continuously variable audio frequency

voltage at a total distortion level of less than 0.1 per cent. This was amplified by a Bogen 75 watt Challenger amplifier. The amplifier output was measured by a John Fluke Model 102 VAW meter and was then introduced into the test section by either a conical or a cylindrical horn coupled to a University type PA-HF speaker driver which had a frequency response of 70 to 10,000 cps. A wave analysis of the resonant acoustic field showed a distortion level of less than one per cent. In order to produce an axially symmetric flow field it was necessary to maintain a very low distortion level in the tube. The driver-horn assembly was rack mounted so that the position of the horn in the tube could be easily varied. This adjustment was very critical, especially for the higher frequencies (960 to 1600 cps). A schematic diagram of the sound generating system is shown in Figure 12.

5. Sound Measuring Equipment. The sound measuring equipment included the following General Radio items:

<u>Item</u>	<u>Type</u>
Sound level meter	1551-A
Power supply	1262-A
High level microphone assembly	1551-PlH
20 db attenuator pad	1551-P 11
Sound level calibrator	1552-B
Transistor oscillator	1307-A

In addition to the General Radio items a Hewlett-Packard Model 302-A wave analyzer with a Hewlett-Packard Model 297-A sweep drive and a Mosley Model 2-D X-Y recorder were used to analyze and record the pressure in the test section.

In order to determine the axial sound pressure distribution in the tube the high level microphone assembly was equipped with a probe and was mounted on a track. A ten turn potentiometer and a dial cord system were used as a direct current voltage input to the X coordinate of the recorder. This voltage varied linearly with the axial position of the probe. The output from the sound level meter was the input to the Y coordinate. Manual movement of the pressure probe resulted in a continuous plot of sound pressure level versus axial position. Figure 14 shows a typical pressure distribution. Wave analyses of the resonant acoustic field showed that the distortion level was less than one per cent.

A Sorensen Model 2501 A-C line voltage regulator supplied the power for all of the electronic equipment.

6. Photographic Equipment. A 4- x 5-inch speed press camera with a Schneider Xenotar 1:2, 3/150 lens and a Polaroid Land Camera back and 3000 speed Polaroid film were used to obtain the photographic data. Both time and flash exposures were used.

2. Experimental Procedure

A warm up time of at least 3 hours was provided for all of the equipment.

After the warm up period the following procedure was followed:

1. The desired flow rate was set up using only the primary air supply (no flow through the smoke generator).
2. The desired resonant frequency was set on the audio signal generator.
3. The amplifier gain was increased until the desired sound level was reached. The maximum sound pressure level was determined by inserting the calibrated probe into the test section.
4. The driver-horn assembly was then adjusted to minimize the driver power. This was a very accurate and simple method of tuning the system. After this, additional fine adjustments in the frequency and the horn position were made until the power reached a relative minimum.
5. The probe was then removed after the maximum sound pressure level was recorded.
6. Photographs of the flow field were taken after allowing sufficient time for steady state conditions to exist.
7. The data that were recorded are: frequency; power supplied to the driver; maximum sound pressure level and flow rate, temperature and pressure of the air.

From the data obtained the vortex size and the value of the parameter \bar{v}/v_0^2 were determined.

CHAPTER IV

DISCUSSION OF RESULTS

At the initiation of this study it was thought that an experimental flat plate geometry would give simpler flow and heat transfer characteristics. Consequently, an analytical and experimental study was initiated utilizing this geometry and its relation to a resonant acoustic sound field. It was believed that the data obtained from the flat plate system would make more and simpler experimental facts available than had previously been obtained with the horizontal tube heat transfer apparatus at Georgia Tech. This reasoning was particularly valid if natural convection was complicating the experimental measurements. Unfortunately, experimental difficulties were encountered with the flat plate system and it was impossible to obtain useful information from it. Some of the reasons for the experimental problems have been given in Chapter III. Preliminary visual exploratory studies with a tube geometry indicated that free convection was not complicating the secondary flow and, therefore, studies were carried out with this system.

It is interesting to note that the theoretical flat plate analysis, limited for the present time to flows without heat transfer, gives some very interesting and useful results and even indicates some plausible explanations of some of the previous experimental data on tube flow. The analytical study also indicates how a similar treatment of the circular geometry can be attempted.

The flow field shown in Figure 7 presents a plausible explanation of the data shown in Figures 1 and 2 and is currently being studied. The maximum local heat transfer rates occur where the main vortex and the main stream impinge upon the wall, i.e. at the velocity loops. The minimum rates occur where both the

vortex and the main stream separate from the wall, i.e. at the velocity nodes.

Another interesting outgrowth of this study was the correlation of the threshold data of Eastwood [2]. Eastwood measured the local heat transfer rate for forced convection in a horizontal isothermal tube with an impressed resonant acoustic field. He defined the sound threshold level to be the sound level below which no noticeable change in the local heat transfer rate occurred. If this is interpreted in terms of the flow field which exists, then it should follow that a certain magnitude of disturbance in the flow would be necessary to produce an observable change in the convection heat transfer characteristics of the tube. From the present theoretical analysis the magnitude of this disturbance should be characterized by the parameter \bar{M}/M_0^2 . Eastwood's threshold data were correlated at a value of (\bar{M}/M_0^2) equal to 63 for the range of average Mach number between 0.005 and 0.017. For Mach numbers less than 0.005 the effect of free convection became appreciable and, therefore, below this value \bar{M}/M_0^2 was not a sufficient description of the flow.

A point which should be emphasized again is that the analytical solution presented herein for channel flow is only valid for values of \bar{M}/M_0^2 less than approximately 10. However, the fact that Eastwood's threshold data correlated for a value of \bar{M}/M_0^2 of 63 indicates that the restriction may be too severe.

It is interesting to note that if the through flow is reduced to zero then the time-mean solution is the same as that predicted by Westervelt [6]. The other extreme case, that of no sound, reduces the solution to one for fully developed laminar channel flow. This condition, however, is not required by the analysis presented here and should be considered as a curiosity rather than a necessity.

Preliminary results of the quantitative visualization experiments with tube flow are shown in Figure 15. The comparison with the theoretical solution for channel flow is interesting. Also the lack of scatter in the experimental data indicates that the parameter, \bar{M}/M_0^2 , is apparently a correlating parameter for tube flow as well as for channel flow. As mentioned previously this parameter correlated Eastwood's heat transfer data for tube flow.

Although differences between the flow patterns of air-oil vapor and air-tobacco smoke were not apparent, qualitative differences did exist. Since the particle size of tobacco smoke is much smaller than that of vaporized oil, only tobacco smoke was used to obtain the quantitative data. Typical flow patterns are shown photographically in Figure 10.

It is anticipated that the solution for the circular duct will be completed by the first of the year and that further improvements in the experimental techniques will permit an accurate verification of this solution.

BIBLIOGRAPHY

1. T. W. Jackson, K. R. Purdy, and C. C. Oliver, "The Effects of Resonant Acoustic Vibrations on the Nusselt Number for a Constant Temperature Horizontal Tube," Second International Heat Transfer Conference, August 1961.
2. Ian Eastwood, T. W. Jackson, C. C. Oliver, and K. R. Purdy, "Heat Transfer Threshold Values for Resonant Acoustic Vibrations in a Horizontal Isothermal Tube," Report on Contract AF 33(616)-8396, January 1962.
3. C. C. Lin, "Motion in the Boundary Layer with a Rapidly Oscillating External Flow," 9th Int. Congress of Applied Mech., University of Brussels, Belgium, 4, September 1956, p. 155.
4. J. V. Sanders, "A Photomultiplier-Schlieren for Acoustic Measurement and Some Investigations of the Kundt's Tube," Dissertation Abstracts, February 1962.
5. Lord Rayleigh, "On the Circulation of Air Observed in Kundt's Tubes and on Some Allied Acoustical Problems," Phil. Trans. of the Royal Soc. of London, 175, Part I, 1884.
6. P. J. Westervelt, "The Theory of Steady Rotational Flow Generated by a Sound Field," Jour. Acoust. Soc. Amer., 25, 1953, pp. 60-67.
7. H. Schlichting, "Berechnung ebener periodischer Grenzschichtströmungen," Phys. Z., 33, 1932, p. 327.
8. P. M. Morse, Vibration and Sound, 2nd ed., New York: McGraw-Hill Book Co., Inc., 1948.
9. E. N. da C. Andrade, "On the Circulation Caused by the Vibrations of Air in a Tube," Proc. of the Royal Soc. (London), Series A, Math and Phy. Soc., 134, 1932, p. 445-70.

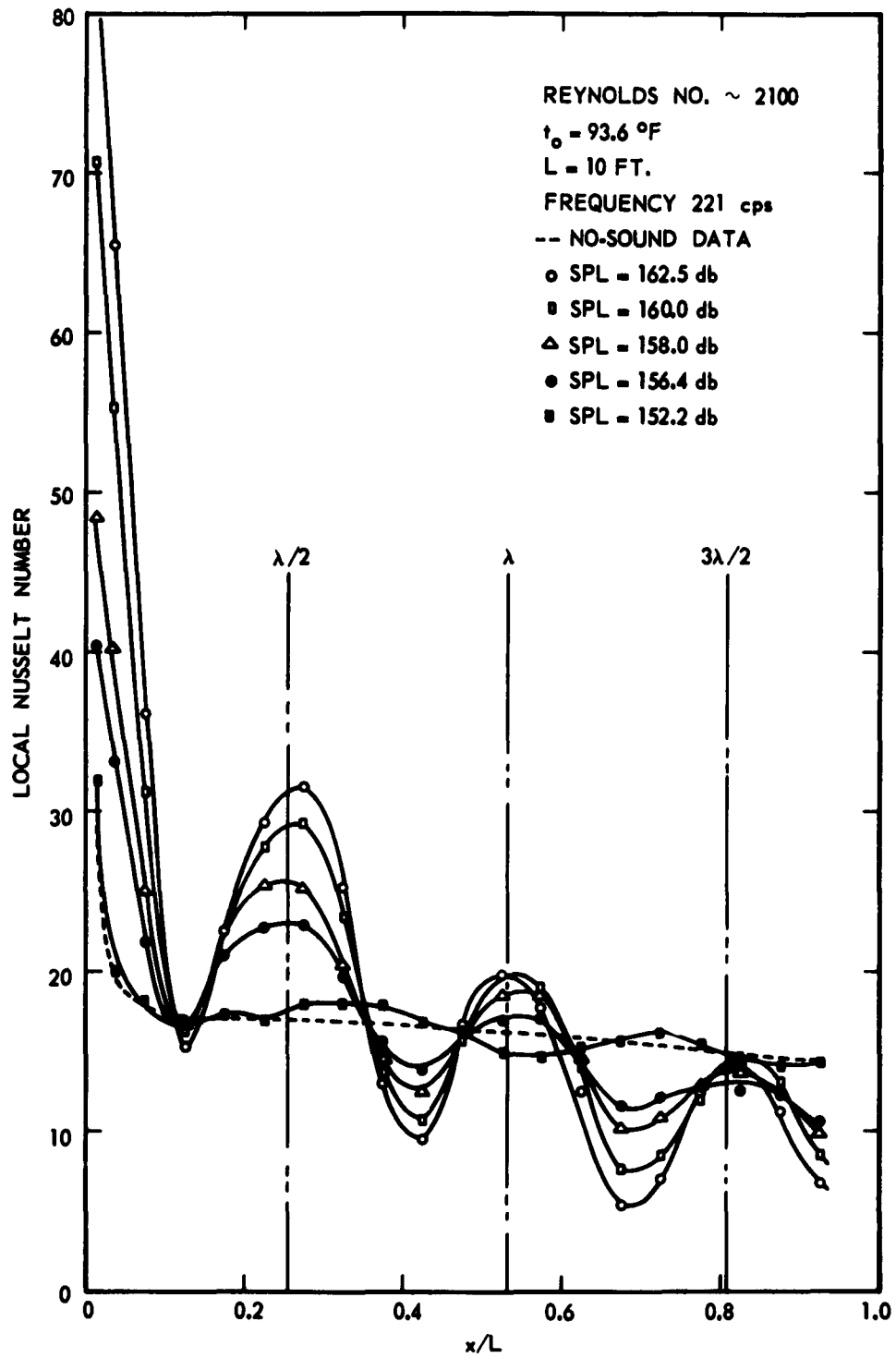


Figure 1. Local Nusselt Numbers Versus x/L for Various Sound Pressure Levels and 221 cps.

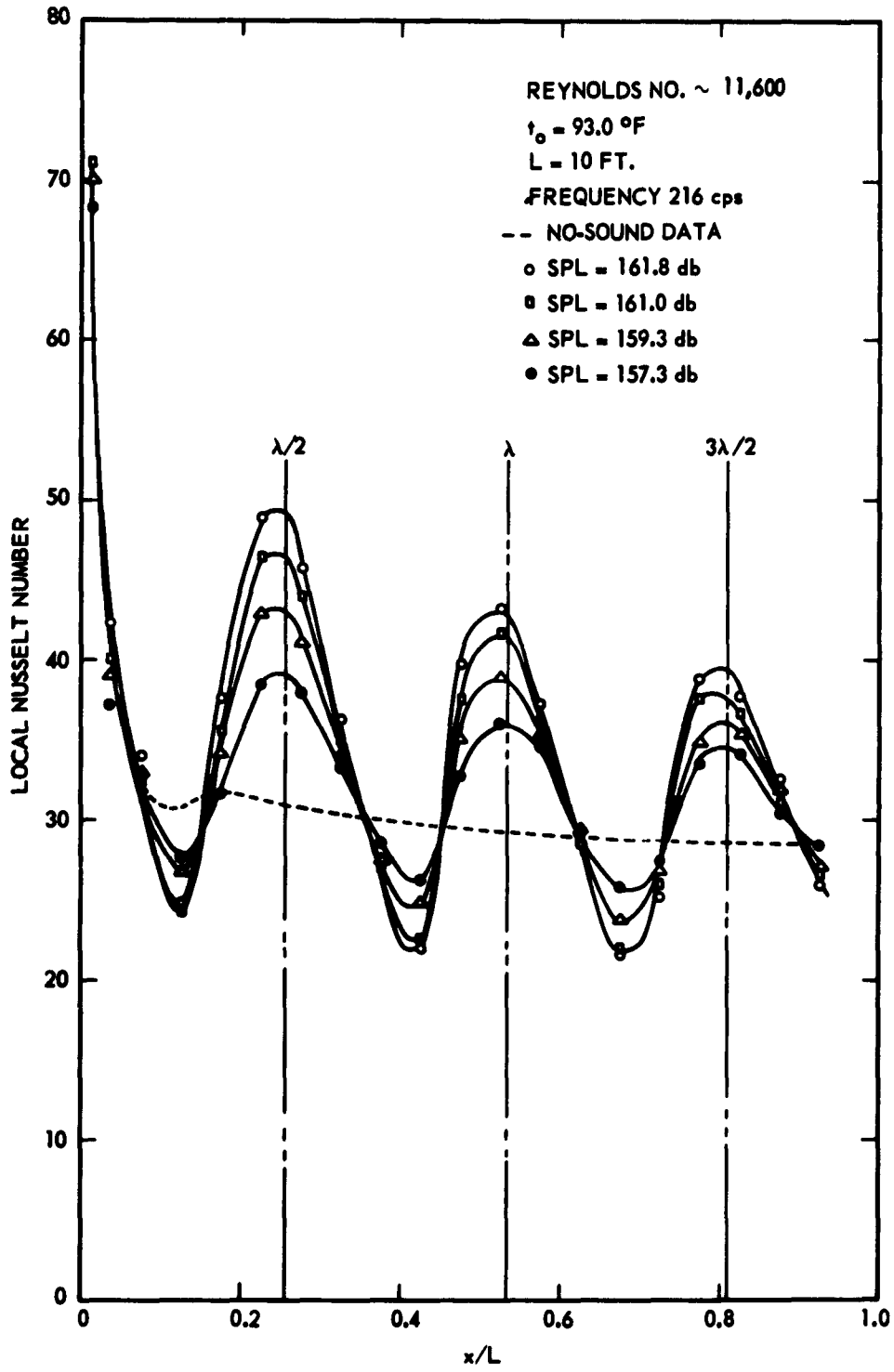


Figure 2. Local Nusselt Numbers Versus x/L for Various Sound Pressure Levels and 216 cps.

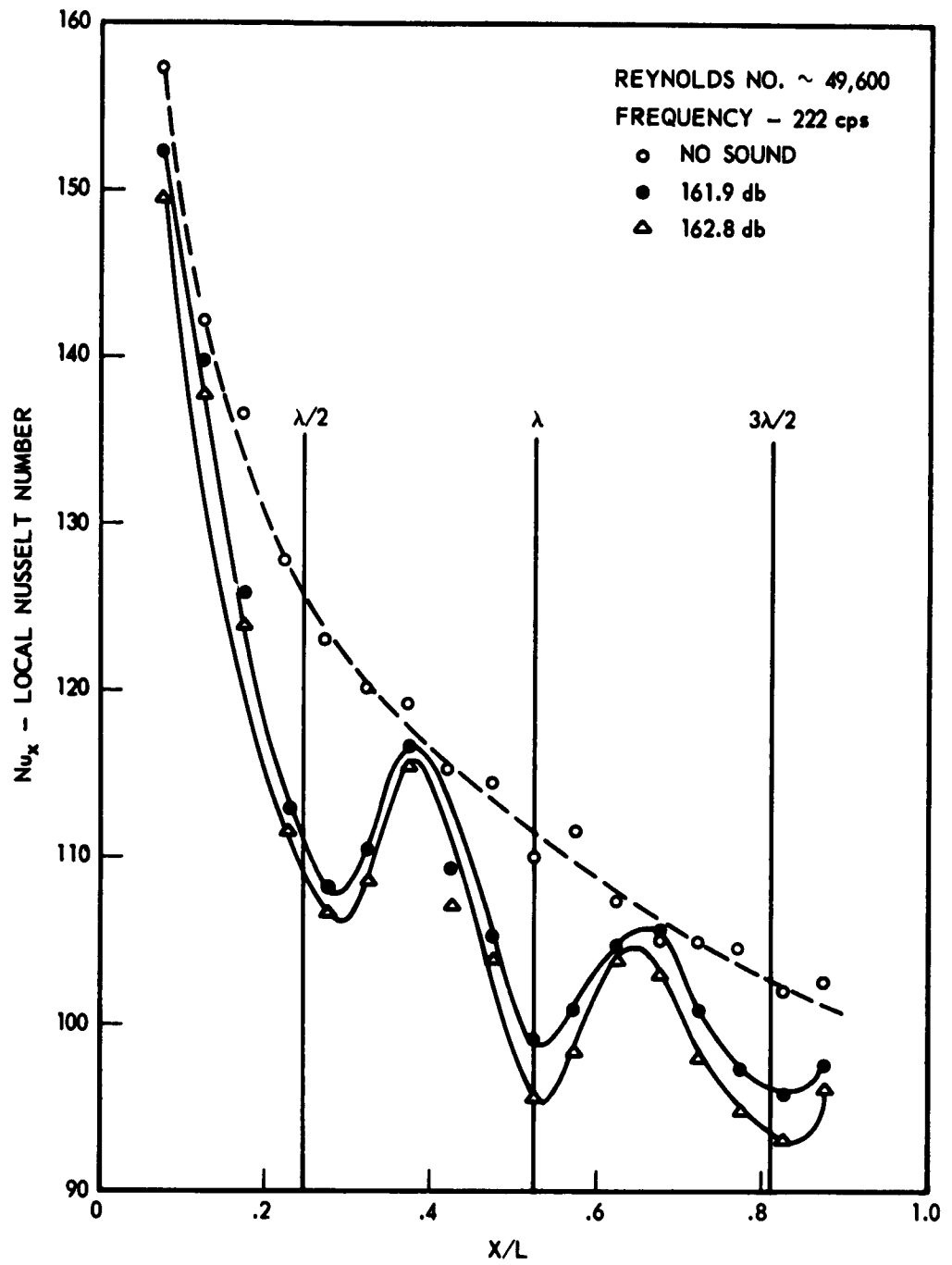


Figure 3. Local Nusselt Numbers Versus x/L for Various Sound Pressure Levels and 222 cps.

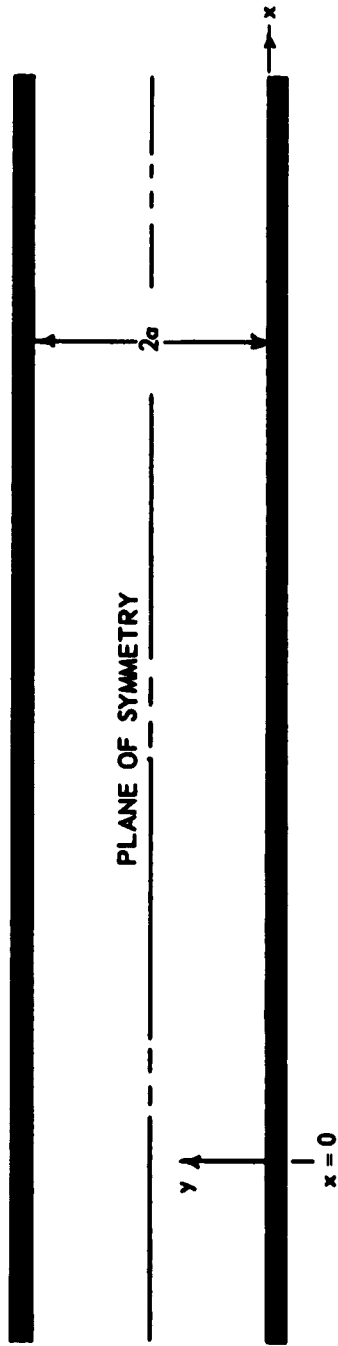


Figure 4. Model of Flow System.

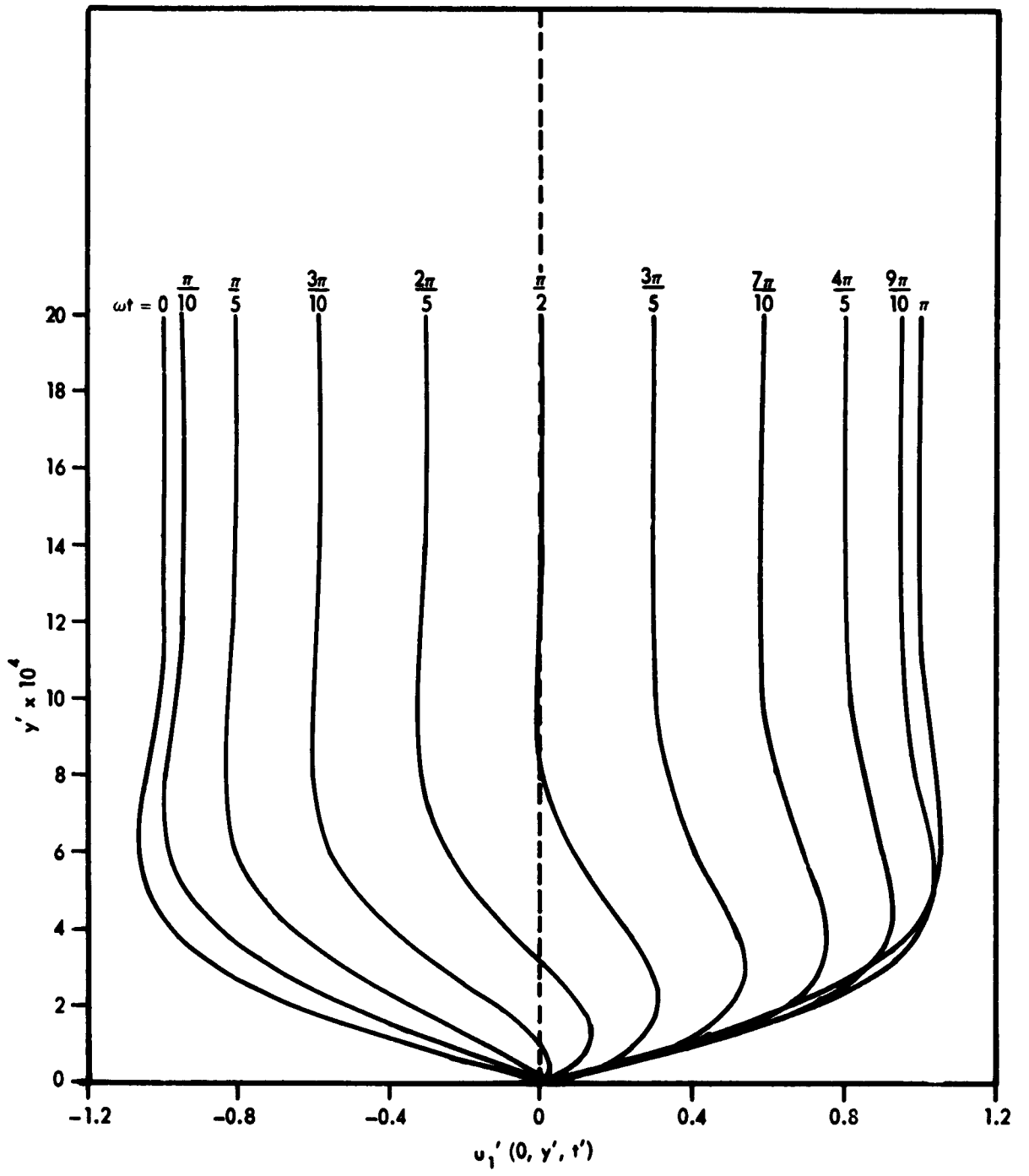


Figure 5. Time Dependent Velocity Profiles.

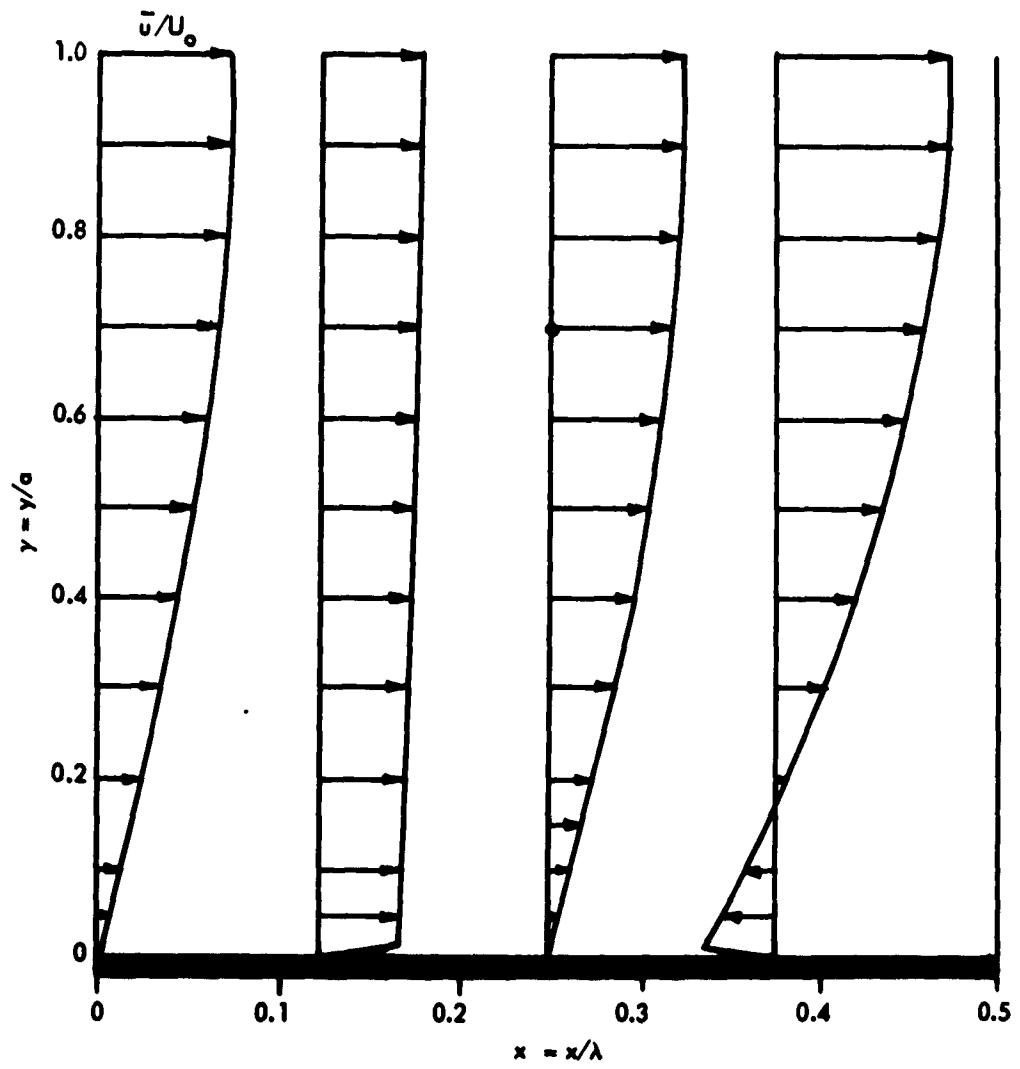


Figure 6. Time Mean Velocity Profiles.

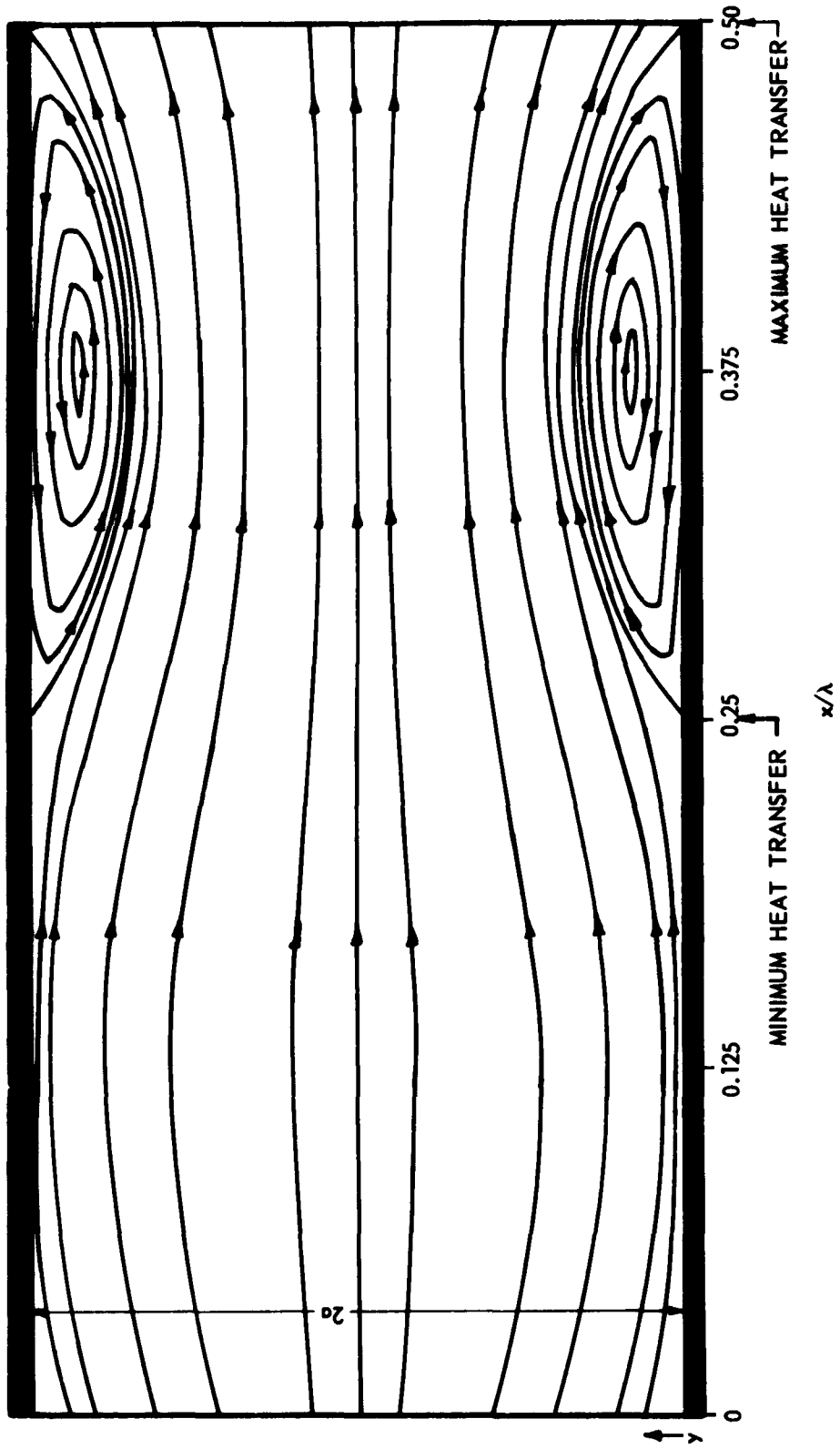


Figure 7. Graphical Representation of Stream Lines.

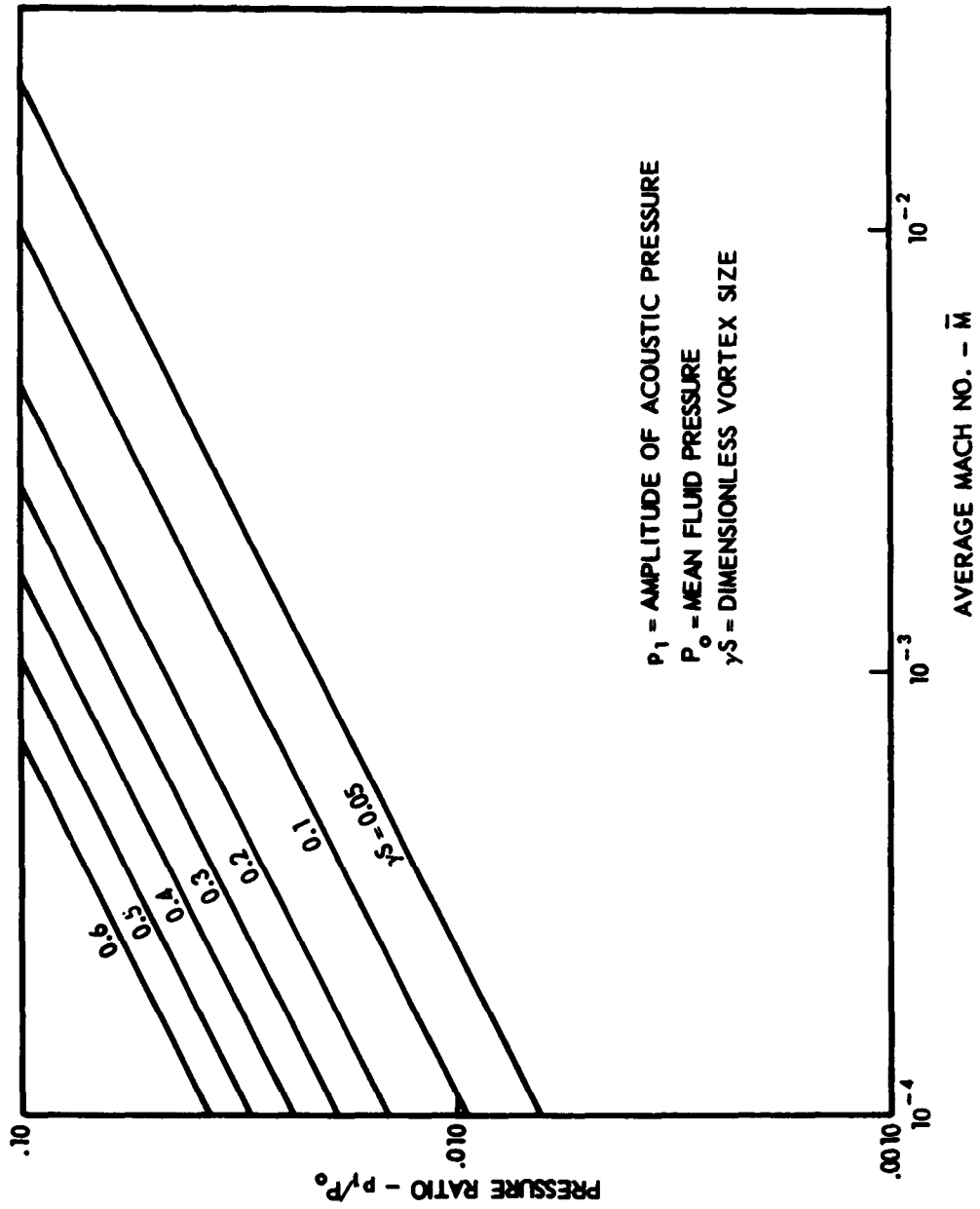


Figure 8. Pressure Disturbance Versus Mean Through Flow Mach Number for Various Vortex Sizes.

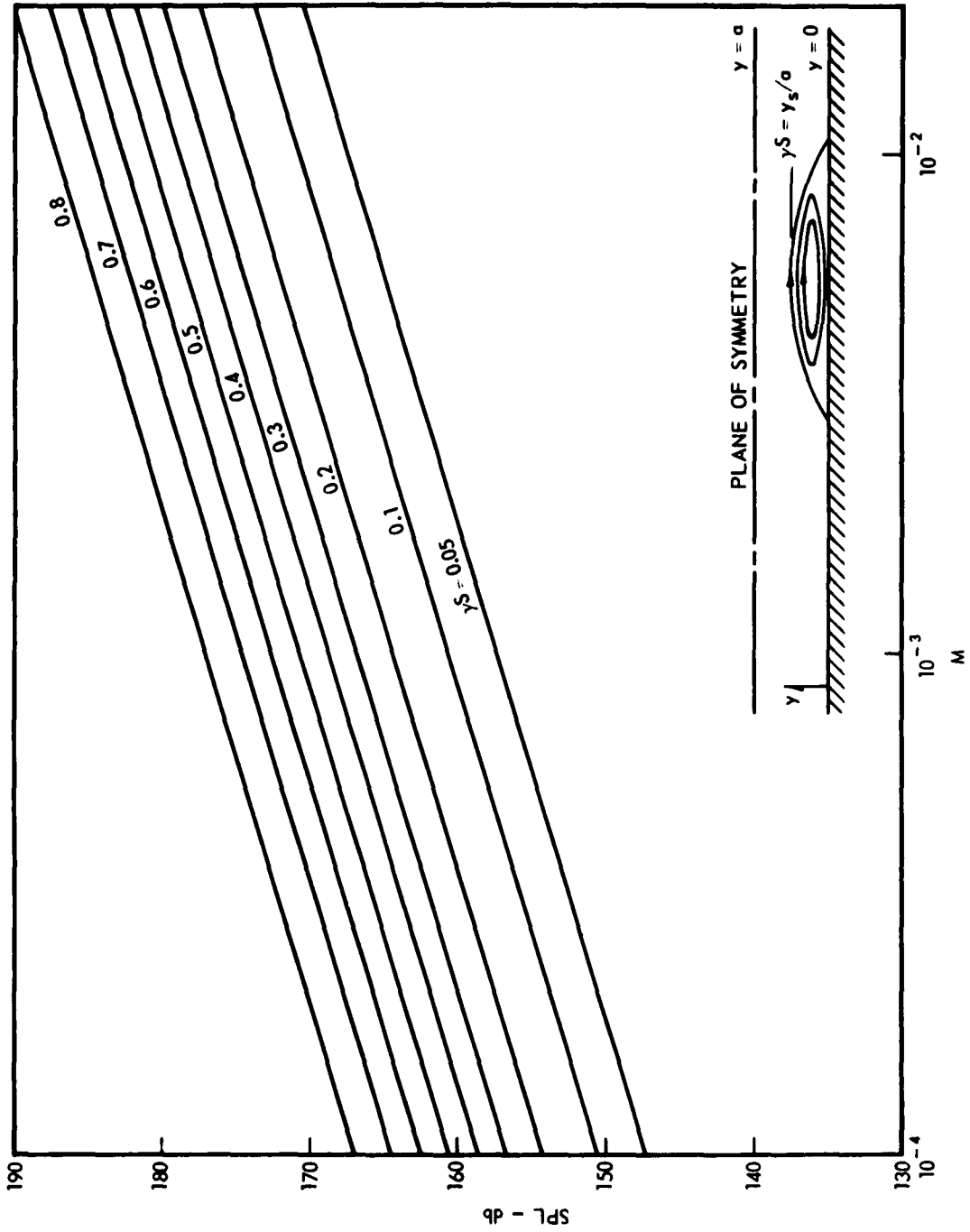
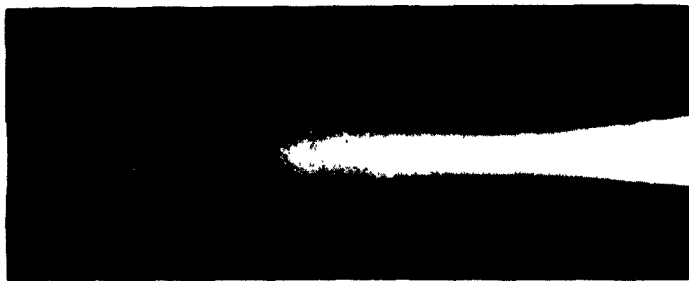


Figure 9. Sound Pressure Level Versus Mean Through Flow Mach Number for Various Vortex Sizes.



←
FLOW

(a) 1440 cps
 $\bar{M} = 1 \times 10^{-4}$



←
FLOW

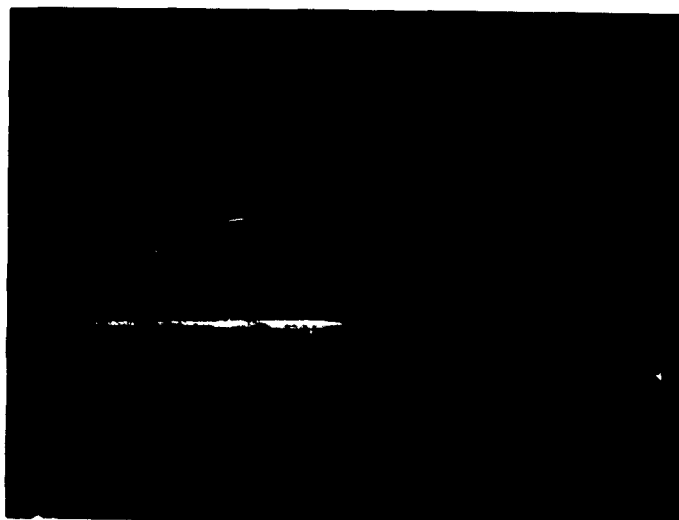
(b) 1600 cps
 $\bar{M} = 1 \times 10^{-4}$



←
FLOW

(c) 1120 cps
 $\bar{M} = 0.5 \times 10^{-4}$

Figure 10. Qualitative Smoke Patterns from Preliminary Investigations for Tube Flow.



←
FLOW

FREQUENCY = 1000 cps
MACH NUMBER = 0.0001

Figure 11. Acoustic Vortices for a Resonant Rectangular Duct.

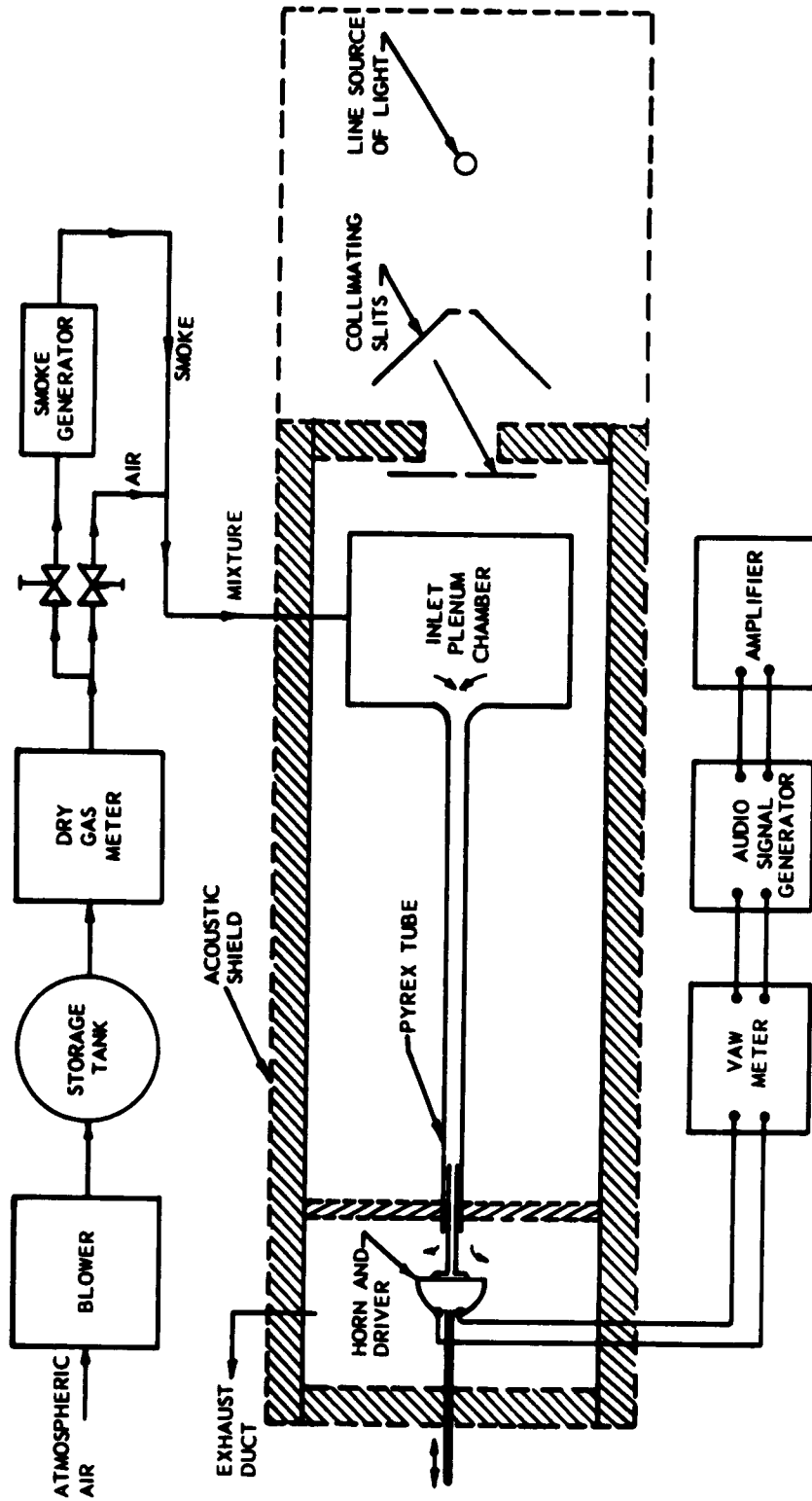


Figure 12. Schematic Diagram of Flow Visualization Equipment.



Figure 13. Photograph of Flow Visualization Apparatus.

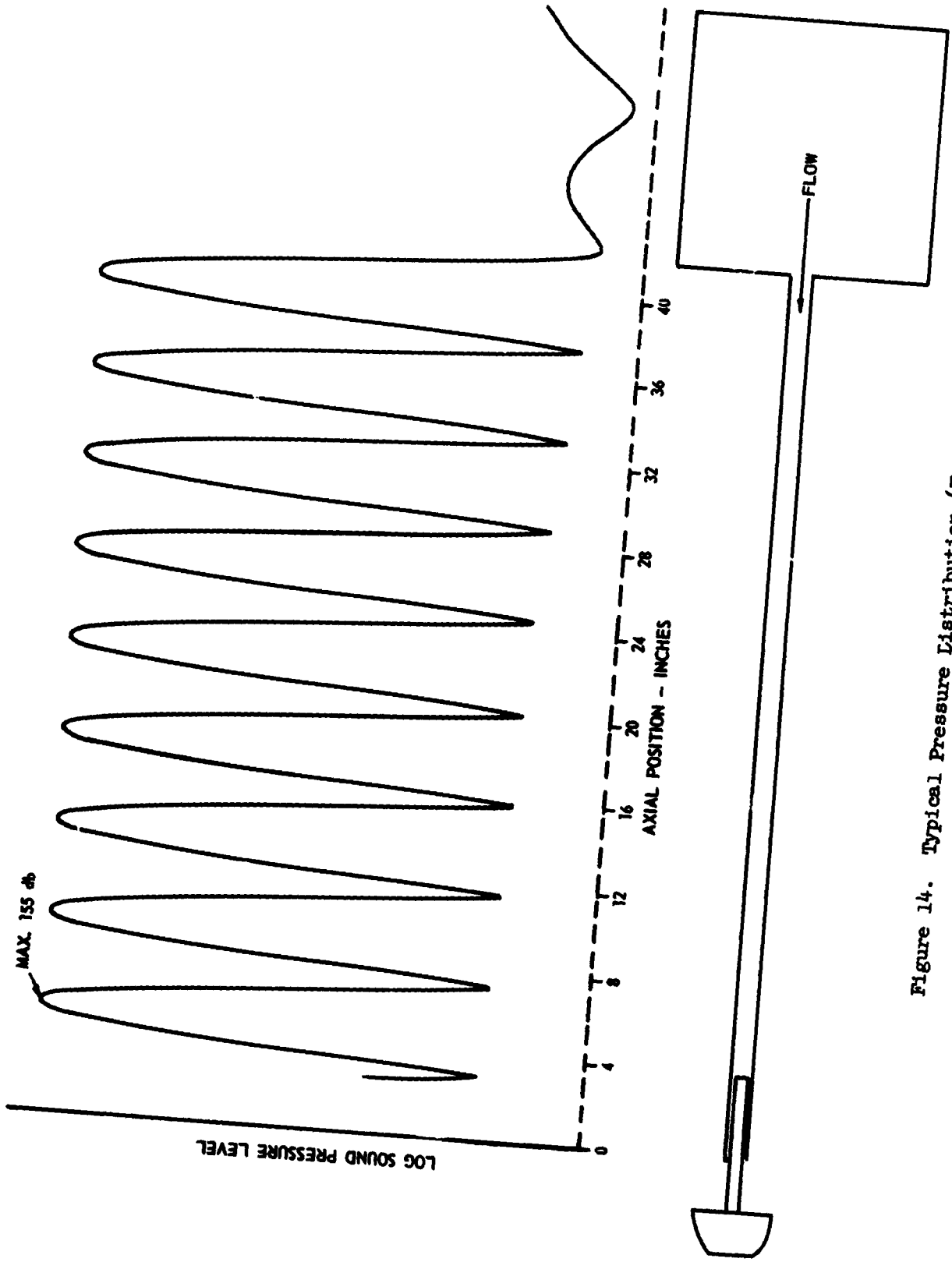


Figure 14. Typical Pressure Distribution (Frequency = 1600 cps).

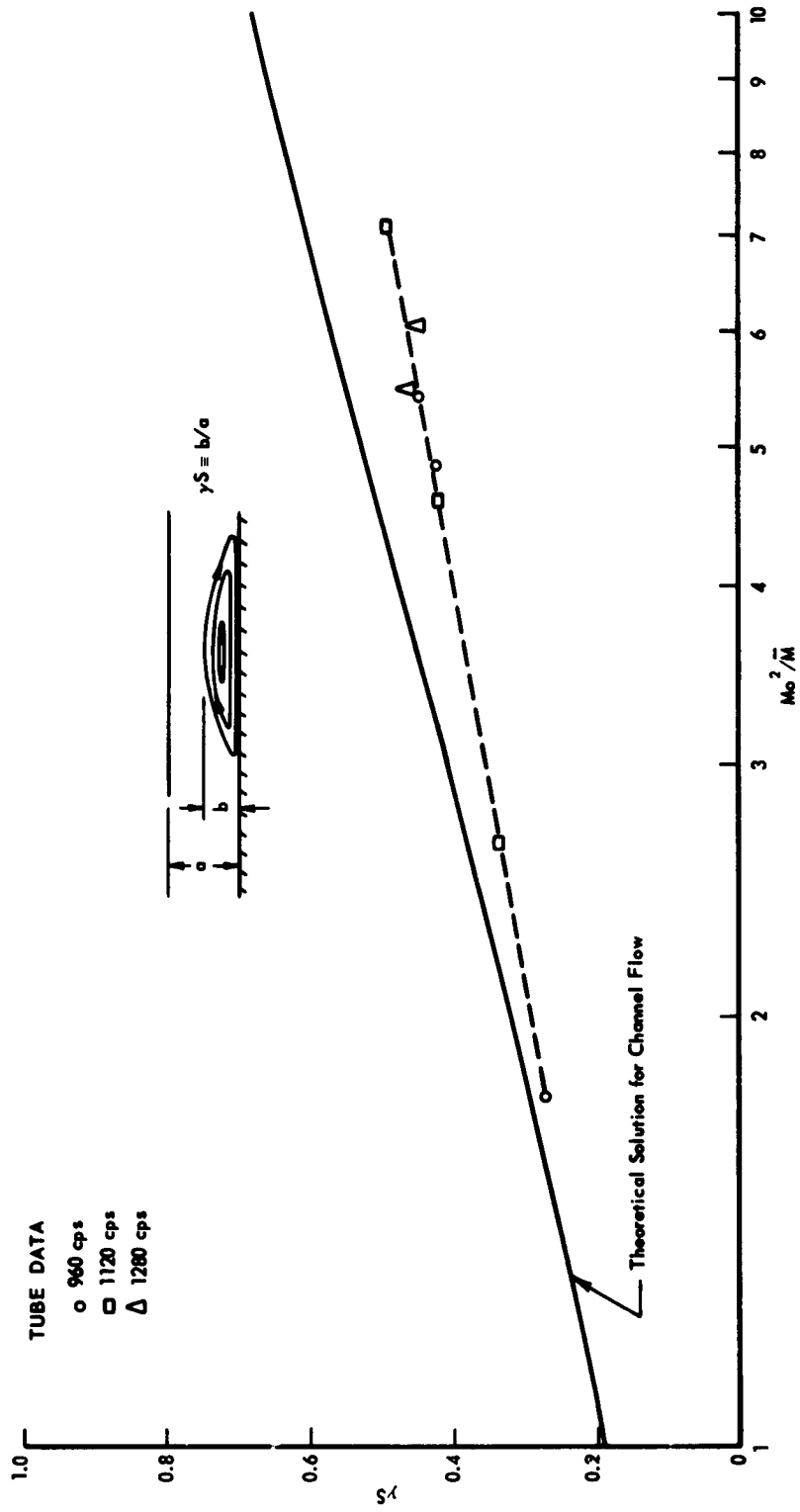


Figure 15. Comparison of Experimental γ_S for Tube with Analytical γ_S for Channel.

UNCLASSIFIED

Aeronautical Research Laboratories, Wright-Patterson AFB, Ohio. VISCOUS COMPRESSIBLE FLUID FLOW UNDER THE INFLUENCE OF A RESONANT ACOUSTIC FIELD by Kenneth R. Purdy, Thomas W. Jackson, Georgia Institute of Technology, Atlanta, Ga. October 1962. 42 p. incl. illus. (Project 7053; Task 7063-01) (Contract AF 33 (616)-8396) (ARL 62-457)

Unclassified Report

This report presents an analytical solution for low Mach number viscous compressible channel flow under the influence of a resonant acoustic field. The solution predicts the existence of standing vortices in the flow and that the ratio of the maximum width

(over)

UNCLASSIFIED

UNCLASSIFIED

Aeronautical Research Laboratories, Wright-Patterson AFB, Ohio. VISCOUS COMPRESSIBLE FLUID FLOW UNDER THE INFLUENCE OF A RESONANT ACOUSTIC FIELD by Kenneth R. Purdy, Thomas W. Jackson, Georgia Institute of Technology, Atlanta, Ga. October 1962. 42 p. incl. illus. (Project 7053; Task 7063-01) (Contract AF 33 (616)-8396) (ARL 62-457)

Unclassified Report

This report presents an analytical solution for low Mach number viscous compressible channel flow under the influence of a resonant acoustic field. The solution predicts the existence of standing vortices in the flow and that the ratio of the maximum width

(over)

UNCLASSIFIED

UNCLASSIFIED

of the vortices to the half width of the channel is solely a function of the parameter M/\bar{M}_0 where \bar{M} is the Mach number based on the average through flow velocity and M_0 is the acoustic Mach number based on the maximum amplitude of the time dependent velocity. The order of magnitude analysis which was used to reduce the equations of motion required that M/\bar{M}_0 should be less than approximately ten. The existence of standing vortices was confirmed experimentally by a visualization study of tube flow. Typical flow fields are shown both graphically and photographically.

(over)

UNCLASSIFIED

of the vortices to the half width of the channel is solely a function of the parameter M/\bar{M}_0 where \bar{M} is the Mach number based on the average through flow velocity and M_0 is the acoustic Mach number based on the maximum amplitude of the time dependent velocity. The order of magnitude analysis which was used to reduce the equations of motion required that M/\bar{M}_0 should be less than approximately ten. The existence of standing vortices was confirmed experimentally by a visualization study of tube flow. Typical flow fields are shown both graphically and photographically.

(over)

UNCLASSIFIED

UNCLASSIFIED

UNCLASSIFIED

Aeronautical Research Laboratories, Wright-Patterson AFB, Ohio. VISCOUS COMPRESSIBLE FLUID FLOW UNDER THE INFLUENCE OF A RESONANT ACOUSTIC FIELD by Kenneth R. Purdy, Thomas W. Jackson, Georgia Institute of Technology, Atlanta, Ga. October 1962. 42 p. incl. illus. (Project 7063; Task 7063-01) (Contract AF 33 (616)-8396) (ARL 62-457)

Unclassified Report

This report presents an analytical solution for low Mach number viscous compressible channel flow under the influence of a resonant acoustic field. The solution predicts the existence of standing vortices in the flow and that the ratio of the maximum width

(over)

UNCLASSIFIED

UNCLASSIFIED

of the vortices to the half width of the channel is solely a function of the parameter M/M_0 where M is the Mach number based on the average through flow velocity and M_0 is the acoustic Mach number based on the maximum amplitude of the time dependent velocity. The order of magnitude analysis which was used to reduce the equations of motion required that M/M_0 should be less than approximately ten. The existence of standing vortices was confirmed experimentally by a visualization study of tube flow. Typical flow fields are shown both graphically and photographically.

(over)

UNCLASSIFIED

UNCLASSIFIED

Aeronautical Research Laboratories, Wright-Patterson AFB, Ohio. VISCOUS COMPRESSIBLE FLUID FLOW UNDER THE INFLUENCE OF A RESONANT ACOUSTIC FIELD by Kenneth R. Purdy, Thomas W. Jackson, Georgia Institute of Technology, Atlanta, Ga. October 1962. 42 p. incl. illus. (Project 7063; Task 7063-01) (Contract AF 33 (616)-8396) (ARL 62-457)

Unclassified Report

This report presents an analytical solution for low Mach number viscous compressible channel flow under the influence of a resonant acoustic field. The solution predicts the existence of standing vortices in the flow and that the ratio of the maximum width

(over)

UNCLASSIFIED

UNCLASSIFIED

of the vortices to the half width of the channel is solely a function of the parameter M/M_0 where M is the Mach number based on the average through flow velocity and M_0 is the acoustic Mach number based on the maximum amplitude of the time dependent velocity. The order of magnitude analysis which was used to reduce the equations of motion required that M/M_0 should be less than approximately ten. The existence of standing vortices was confirmed experimentally by a visualization study of tube flow. Typical flow fields are shown both graphically and photographically.

(over)

UNCLASSIFIED